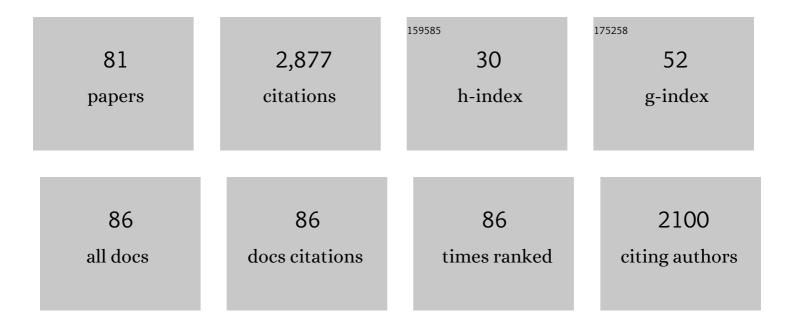
List of Publications by Year in descending order

Source: https://exaly.com/author-pdf/8506220/publications.pdf

Version: 2024-02-01



#	Article	IF	CITATIONS
1	High-Pressure Creep of Serpentine, Interseismic Deformation, and Initiation of Subduction. Science, 2007, 318, 1910-1913.	12.6	331
2	Deformation of polycrystalline MgO at pressures of the lower mantle. Journal of Geophysical Research, 2002, 107, ECV 3-1-ECV 3-17.	3.3	207
3	Plastic Deformation of MgGeO3 Post-Perovskite at Lower Mantle Pressures. Science, 2006, 311, 644-646.	12.6	143
4	Deformation of (Mg,Fe)SiO3 Post-Perovskite and D'' Anisotropy. Science, 2007, 316, 1729-1732.	12.6	139
5	Raman Spectroscopy of Iron to 152 Gigapascals: Implications for Earth's Inner Core. Science, 2000, 288, 1626-1629.	12.6	130
6	Deformation of (Mg0.9,Fe0.1)SiO3 Perovskite aggregates up to 32 GPa. Earth and Planetary Science Letters, 2003, 209, 351-360.	4.4	88
7	X-ray transparent gasket for diamond anvil cell high pressure experiments. Review of Scientific Instruments, 2005, 76, 046109.	1.3	79
8	Finite-element modeling of diamond deformation at multimegabar pressures. Applied Physics Letters, 1999, 74, 656-658.	3.3	75
9	Deformation of polycrystalline iron up to 30GPa and 1000K. Physics of the Earth and Planetary Interiors, 2004, 145, 239-251.	1.9	72
10	Single-crystal diffraction at the Extreme Conditions beamline P02.2: procedure for collecting and analyzing high-pressure single-crystal data. Journal of Synchrotron Radiation, 2013, 20, 711-720.	2.4	67
11	Modeling analysis of the influence of plasticity on high pressure deformation of hcp-Co. Physical Review B, 2009, 79, .	3.2	66
12	Dislocations and Plastic Deformation in MgO Crystals: A Review. Crystals, 2018, 8, 240.	2.2	62
13	Aggregate and single-crystalline elasticity of hcp cobalt at high pressure. Physical Review B, 2005, 72, .	3.2	59
14	Equation of state, elasticity, and shear strength of pyrite under high pressure. Physics and Chemistry of Minerals, 2002, 29, 1-9.	0.8	53
15	Mechanism of the <mml:math xmlns:mml="http://www.w3.org/1998/Math/MathML"><mml:mrow><mml:mi>α</mml:mi><mml:mo>â^'transformation in iron. Physical Review B, 2015, 91, .</mml:mo></mml:mrow></mml:math 	l:mo s. 2mml	:mi ɛû u
16	Lattice preferred orientation and stress in polycrystalline hcp-Co plastically deformed under high pressure. Journal of Applied Physics, 2006, 100, 023510.	2.5	44
17	Experimental method for <i>in situ</i> determination of material textures at simultaneous high pressure and high temperature by means of radial diffraction in the diamond anvil cell. Review of Scientific Instruments, 2009, 80, 104501.	1.3	43
18	Deformation textures produced in diamond anvil experiments, analysed in radial diffraction geometry. Journal of Physics Condensed Matter, 2006, 18, S933-S947.	1.8	42

#	Article	IF	CITATIONS
19	High resolution threeâ€dimensional Xâ€ray diffraction study of dislocations in grains of MgGeO ₃ postâ€perovskite at 90 GPa. Journal of Geophysical Research, 2012, 117, .	3.3	42
20	Lattice preferred orientation in CalrO3 perovskite and post-perovskite formed by plastic deformation under pressure. Physics and Chemistry of Minerals, 2007, 34, 679-686.	0.8	41
21	Effects of texture on the determination of elasticity of polycrystalline ϵ-iron from diffraction measurements. Earth and Planetary Science Letters, 2001, 194, 201-212.	4.4	40
22	Elastic anisotropy in hcp metals at high pressure and the sound wave anisotropy of the Earth's inner core. Geophysical Research Letters, 2006, 33, .	4.0	39
23	Axial temperature gradient and stress measurements in the deformation-DIA cell using alumina pistons. Review of Scientific Instruments, 2013, 84, 043906.	1.3	39
24	A new high-pressure form of KAlSi3O8under lower mantle conditions. Geophysical Research Letters, 2004, 31, .	4.0	38
25	X-ray diffraction study of the single-crystal elastic moduli of ε-Fe up to 30 GPa. Journal of Geophysical Research, 2005, 110, .	3.3	37
26	Equation of state and phase transition in KAlSi3O8 hollandite at high pressure. American Mineralogist, 2006, 91, 327-332.	1.9	37
27	In situ radial X-ray diffraction study of texture and stress during phase transformations in bcc-, fcc- and hcp-iron up to 36 GPa and 1000 K. Acta Materialia, 2013, 61, 5144-5151.	7.9	37
28	Deformation Behavior across the Zircon-Scheelite Phase Transition. Physical Review Letters, 2016, 117, 135701.	7.8	37
29	Deformation of olivine under mantle conditions: An in situ highâ€pressure, highâ€ŧemperature study using monochromatic synchrotron radiation. Journal of Geophysical Research, 2012, 117, .	3.3	34
30	A Physical Basis for Time Clustering of Large Earthquakes. Bulletin of the Seismological Society of America, 2001, 91, 1685-1693.	2.3	32
31	X-ray diffraction evaluation of stress in high pressure deformation experiments. Journal of Physics Condensed Matter, 2006, 18, S949-S962.	1.8	30
32	Texture development and elastic stresses in magnesiowűstite at high pressure. Physics and Chemistry of Minerals, 2006, 33, 84-97.	0.8	29
33	Texture and elastic strains in hcp-iron plastically deformed up to 17.5 GPa and 600 K: experiment and model. Modelling and Simulation in Materials Science and Engineering, 2012, 20, 024005.	2.0	27
34	Microstructures and rheology of the Earth's upper mantle inferred from a multiscale approach. Comptes Rendus Physique, 2010, 11, 304-315.	0.9	26
35	Significance of mechanical twinning in hexagonal metals at high pressure. Acta Materialia, 2012, 60, 430-442.	7.9	26
36	Evidence for {100}<011> slip in ferropericlase in Earth's lower mantle from high-pressure/high-temperature experiments. Earth and Planetary Science Letters, 2018, 489, 251-257.	4.4	26

#	Article	IF	CITATIONS
37	<i>In situ</i> rheological measurements at extreme pressure and temperature using synchrotron X-ray diffraction and radiography. Journal of Synchrotron Radiation, 2009, 16, 748-756.	2.4	25
38	Diamond anvil cell deformation of CaSiO3 perovskite up to 49GPa. Physics of the Earth and Planetary Interiors, 2009, 174, 159-164.	1.9	25
39	Deformation of MnGeO ₃ postâ€perovskite at lower mantle pressure and temperature. Geophysical Research Letters, 2010, 37, .	4.0	24
40	<i>Multifit</i> / <i>Polydefix</i> : a framework for the analysis of polycrystal deformation using X-rays. Journal of Applied Crystallography, 2015, 48, 1307-1313.	4.5	23
41	Kinetic D/H fractionation during hydration and dehydration of silicate glasses, melts and nominally anhydrous minerals. Geochimica Et Cosmochimica Acta, 2018, 233, 14-32.	3.9	23
42	Microstructural effects and mechanism of bcc-hcp-bcc transformations in polycrystalline iron. Physical Review B, 2020, 102, .	3.2	23
43	Quantitative Rietveld texture analysis of CaSiO3perovskite deformed in a diamond anvil cell. Journal of Physics Condensed Matter, 2006, 18, S995-S1005.	1.8	21
44	Novel experimental setup for megahertz X-ray diffraction in a diamond anvil cell at the High Energy Density (HED) instrument of the European X-ray Free-Electron Laser (EuXFEL). Journal of Synchrotron Radiation, 2021, 28, 688-706.	2.4	21
45	Femtosecond Visualization of hcp-Iron Strength and Plasticity under Shock Compression. Physical Review Letters, 2021, 127, 205501.	7.8	21
46	Texturing in Earth's inner core due to preferential growth in its equatorial belt. Physics of the Earth and Planetary Interiors, 2011, 188, 173-184.	1.9	20
47	Elasto-viscoplastic self consistent modeling of the ambient temperature plastic behavior of periclase deformed up to 5.4 GPa. Journal of Applied Physics, 2017, 122, .	2.5	20
48	Shear wave anisotropy in textured phase D and constraints on deep water recycling in subduction zones. Earth and Planetary Science Letters, 2013, 377-378, 13-22.	4.4	17
49	Effective viscoplastic behavior of polycrystalline aggregates lacking four independent slip systems inferred from homogenization methods; application to olivine. Journal of the Mechanics and Physics of Solids, 2015, 83, 199-220.	4.8	17
50	Multiscale model of global inner ore anisotropy induced by hcp alloy plasticity. Geophysical Research Letters, 2016, 43, 1084-1091.	4.0	17
51	<i>In situ</i> quantitative analysis of stress and texture development in forsterite aggregates deformed at 6â€GPa and 1373â€K. Journal of Applied Crystallography, 2012, 45, 263-271.	4.5	15
52	Multiscale modeling of upper mantle plasticity: From single-crystal rheology to multiphase aggregate deformation. Physics of the Earth and Planetary Interiors, 2014, 228, 232-243.	1.9	15
53	Is inner core seismic anisotropy a marker for plastic flow of cubic iron?. Geophysical Research Letters, 2015, 42, 1326-1333.	4.0	15
54	Deformation of forsterite polycrystals at mantle pressure: Comparison with Fe-bearing olivine and the effect of iron on its plasticity. Physics of the Earth and Planetary Interiors, 2015, 240, 95-104.	1.9	15

#	Article	IF	CITATIONS
55	<i>In situ</i> monitoring of phase transformation microstructures at Earth's mantle pressure and temperature using multi-grain XRD. Journal of Applied Crystallography, 2015, 48, 1346-1354.	4.5	15
56	Three-dimensional X-ray diffraction in the diamond anvil cell: application to stishovite. High Pressure Research, 2014, 34, 158-166.	1.2	14
57	Evolution of grain sizes and orientations during phase transitions in hydrous Mg ₂ SiO ₄ . Journal of Geophysical Research: Solid Earth, 2016, 121, 7161-7176.	3.4	14
58	X-ray Free Electron Laser-Induced Synthesis of ε-Iron Nitride at High Pressures. Journal of Physical Chemistry Letters, 2021, 12, 3246-3252.	4.6	14
59	Polycrystalline olivine rheology in dislocation creep: Revisiting experimental data to 8.1GPa. Physics of the Earth and Planetary Interiors, 2014, 228, 211-219.	1.9	13
60	An improved setup for radial diffraction experiments at high pressures and high temperatures in a resistive graphite-heated diamond anvil cell. Review of Scientific Instruments, 2020, 91, 045121.	1.3	11
61	Seismic response and anisotropy of a model hcp iron inner core. Comptes Rendus - Geoscience, 2014, 346, 148-157.	1.2	10
62	Effect of lattice preferred orientation on lattice strains in polycrystalline materials deformed under high pressure: Application to hcp-Co. Journal of Physics and Chemistry of Solids, 2006, 67, 2119-2131.	4.0	9
63	Kinetics and detectability of the bridgmanite to post-perovskite transformation in the Earth's D″ layer. Nature Communications, 2019, 10, 5680.	12.8	8
64	Amorphous boron composite gaskets for <i>in situ</i> high-pressure and high-temperature studies. High Pressure Research, 2016, 36, 564-574.	1.2	7
65	Reliability of multigrain indexing for orthorhombic polycrystals above 1â€Mbar: application to MgSiO ₃ post-perovskite. Journal of Applied Crystallography, 2017, 50, 120-130.	4.5	7
66	Detecting seismic anisotropy above the 410†km discontinuity using reflection coefficients of underside reflections. Physics of the Earth and Planetary Interiors, 2018, 274, 170-183.	1.9	7
67	High-pressure yield strength of rocksalt structures using quartz Raman piezometry. Comptes Rendus - Geoscience, 2019, 351, 71-79.	1.2	4
68	Radial Diffraction in the Diamond Anvil Cell: Methods and Applications. NATO Science for Peace and Security Series B: Physics and Biophysics, 2010, , 111-122.	0.3	4
69	The mantle deformed. Nature, 2004, 428, 812-813.	27.8	3
70	Textures in deforming forsterite aggregates up to 8ÂGPa and 1673ÂK. Physics and Chemistry of Minerals, 2016, 43, 409-417.	0.8	2
71	The equation of state of TaC0.99 by X-ray diffraction in radial scattering geometry to 32 GPa and 1073 K Journal of Applied Physics, 2019, 126, .		2
72	Olivine intergranular plasticity at mantle pressures and temperatures. Comptes Rendus - Geoscience, 2019, 351, 80-85.	1.2	2

#	Article	IF	CITATIONS
73	High pressure exploration in the Li–Ln–V–O system. Dalton Transactions, 2020, 49, 13663-13670.	3.3	2
74	Plastic deformation of minerals at high pressure. , 0, , 339-355.		2
75	Deformation of NaCoF ₃ perovskite and post-perovskite up to 30 CPa and 1013 K: implications for plastic deformation and transformation mechanism. European Journal of Mineralogy, 2021, 33, 591-603.	1.3	1
76	Deformation of Polycrystalline MgO Up to 8.3ÂGPa and 1270ÂK: Microstructures, Dominant Slip-Systems, and Transition to Grain Boundary Sliding. Frontiers in Earth Science, 2022, 10, .	1.8	1
77	Corrigendum to "Deformation of polycrystalline iron up to 30 GPa and 1000 K―[Phys. Earth Planet Inter. 145 (2004) 239–251]. Physics of the Earth and Planetary Interiors, 2005, 150, 351-352.	1.9	Ο
78	Earth's inner weakness. Nature Geoscience, 2013, 6, 514-515.	12.9	0
79	Earth's inner core. Comptes Rendus - Geoscience, 2014, 346, .	1.2	Ο
80	Ultrafast X-ray Diffraction Study of a Shock-Compressed Iron Meteorite above 100 GPa. Minerals (Basel, Switzerland), 2021, 11, 567.	2.0	0
81	Deformation and slip systems of <mml:math xmlns:mml="http://www.w3.org/1998/Math/MathML"> <mml:msub> <mml:mi>CaCl </mml:mi> <mml:mn>2 -type <mml:math xmlns:mml="http://www.w3.org/1998/Math/MathML"> <mml:msub> <mml:mi>MnO </mml:mi> <mml:mn>2 <td>2.4</td><td>0</td></mml:mn></mml:msub></mml:math </mml:mn></mml:msub></mml:math 	2.4	0